RSC Advances

ROYAL SOCIETY OF CHEMISTRY

www.rsc.org/advances

Quick and simple integration of optical oxygen sensors into glass-based microfluidic devices*

Liliana C. Lasave, Sergey M. Borisov, Josef Ehgartner, Torsten Mayr†

This work presents a novel simple and inexpensive technique for integration of optical oxygen sensors into microfluidic chips made of glass. The channels of chips are coated with conjugated polymeric nanoparticles containing a covalently grafted oxygen indicator. The resulting layer of physically adsorbed nanoparticles shows excellent stability in buffers of various pH and in presence of a surfactant without noticeable leaching. The integrated sensors feature ultrafast response (less than 0.2 seconds) and repeatable quenching behavior when exposed to different concentrations of oxygen present in air or aqueous solutions. They can be read-out either in lifetime or in ratiometric intensity modalities using unsophisticated, compact and low-cost fluorescence detection systems such as a dual RGB/NIR camera or a phase fluorometer. We also present a new technique for modification of smooth glass surfaces based on *in situ* generation and deposition of dense silica microparticles, which act as an adsorbent for the oxygen-sensitive nanoparticles. This modification dramatically improves the loading with the nanoparticles due to increased surface roughness and maximized contact surface area. Finally, packed-bed micro reactors with integrated oxygen-sensing layers and filled with silica beads containing the enzyme immobilized on its surface are demonstrated to have high potential for investigation of enzymatic activity.

* Electronic supplementary information (ESI) available

† Institute of Analytical Chemistry and Food Chemistry, Graz University of Technology, Stremayrgasse 9/II, 8010 Graz, Austria. E-mail: torsten.mayr@tugraz.at

Introduction

Many chemical and biochemical processes require the presence of oxygen as a reactant to occur. In particular, numerous applications in different areas varying from biological and medical research to food and waste management industries, require continuous and accurate monitoring of oxygen, especially in dissolved form.[1, 2]

Microfluidics is an interdisciplinary field characterized by development of fluid handling systems at the sub-millimeter scale which allows improved analytical performance trough fast analysis, reduction of reagent consumption, increasing reliability and sensitivity through automation, and integrating multiple processes in single devices. This technology is replacing traditional strategies of analysis in diagnostics and biology research.[3, 4, 5] The materials used to fabricate microfluidic devices belong to three broad groups: inorganic, polymeric or paper-based.[6, 7, 8] Although different sensing strategies can be used to quantify oxygen, the optical detection proved to be the most attractive and reliable method. This is due to the fact that optical oxygen sensors can be used for measurement both in gas and in liquid phase, are typically inexpensive, easy to miniaturize, can be used remotely, are non-invasive and do not suffer from electrical interferences nor consume oxygen.[9, 10] Optical oxygen sensors rely on quenching of luminescence of an indicator by molecular oxygen, which results in a decrease of both the luminescence intensity and the decay time.[9] Therefore, it is essential that the material of the chip (i) is not permeable to this gas, (ii) does not show autofluorescence and (iii) is transparent to visible and near-infrared light. Glass combines all these qualities and is therefore a material of choice for such an application.[11]

Integrating sensors into microfabricated devices could have broad implications for the utility and widespread adoption of these systems.[12,13] Planar sensor layer are the most common format of optical sensors applied in microfluidics. They can be deposited from a so-called 'sensor cocktail' (polymer matrix material, indicator and additives dissolved in a suitable solvent) onto a substrate by spin coating, screen printing, pipetting or knife coating.[14] Structuring was achieved by removing unwanted bulk material by various techniques[15,16,17] or photopatterning.[18] Recent reports explore inkjet or pin-printing.[19,20] These techniques are generally applied to modify opened micro-channel surfaces which in a further step must be closed using a lid of some other transparent material such as glass or organic polymers.[21] Herein, the sensor coating has to withstand the relatively harsh conditions of glass bonding procedures

including high temperatures and cleaning. Coating of assembled microfluidic chips, however, remains very challenging due to the small dimension of the channels. It is difficult to obtain homogeneous layers inside the channels and avoid clotting and occlusion. In situ generation of a sensor spot using magnetic nano- or microparticles represents an elegant approach[22] but it requires integration of the magnet into the set-up which may not always be convenient. That is why development of new fast, simple and low-cost techniques for integration of oxygen sensors into microfluidic devices is of great importance.

In this paper we describe a novel method which relies on physical adsorption of oxygen-sensitive nanoparticles onto the glass surface of micro-channels. It will be demonstrated that such modification results in stable and bright oxygen-sensitive coating which can be read-out with different techniques. Additionally, we propose a single step sol-gel technique based on in situ generation and deposition of silica microparticles on smooth glass surfaces resulting in increased roughness and enhanced adsorbent properties of such chips. Finally, this study suggests possible applications of the developed techniques for the study of enzyme activity using packed-bed reactors filled with silica beads containing the enzyme immobilized on its surface.

Materials and methods

Materials

Powder-blasted microfluidic chips and polished glass chip of 1 mm diameter channel (packed-bed reactors) were custom ordered from ix-factory (Dortmund, Germany, ix-factory.de). Powder-blasted meander glass chips of 0.15 mm diameter channel were purchased from Micronit Microfluidics (Enschede, the Netherlands, www.micronit.com).

Oxygen-sensitive conjugated polymer nanoparticles were prepared as previously reported by Dmitriev and collaborators.[23] Type I nanoparticles (C = 0.8 mg/mL) were based on polyfluorene with grafted Pt(II) meso-di(pentafluorophenyl)diphenylporphyrin whereas the Type II nanoparticles (C = 1mg/mL) included the alternating polymer of polyfluorene and benzothiadiazole and grafted Pt(II) benzoporphyrin (Fig. S1). The aqueous dispersions of the nanoparticles were stored in refrigerator at 4 °C until use.

Tetraethoxysilane (TEOS) was acquired from Fluka and acetic acid from Roth (www.carlroth.com).

Integration of the nanoparticles into powder-blasted chips

The channels of microfluidic chips were filled with aqueous dispersion of the nanoparticles and the chips were kept overnight at room temperature in a desiccator with 100% relative humidity. The chips were washed with deionized water and dried under a flow of nitrogen (Linde Gas, Austria; www.linde.at).

Modification of the polished-glass surfaces

First, 1.9 mL of TEOS was added under vigorous stirring into a mixture of 2 mL of glacial acetic acid and 0.6 mL of deionized water. The resulted solution was immediately injected into the channels of a packed-bed microfluidic chip. After 20 min the channel was exhaustively washed with deionized water, dried under a flux of compressed air and further dried in an oven at 100 °C for several hours. The oxygen-sensitive nanoparticles were integrated as described for the powder-blasted chips.

Measurements

SEM images were acquired on a ZEISS Ultra-55 Scanning Electron Microscope (Zeiss, Germany) using an In-Lens and secondary electrons (SE) and backscattered electron (BSE) detectors. Images of the channels of microfluidic chips were taken with the optical microscope (Zeiss Axiovert 25 CFL).

Single point phosphorescence lifetime measurement

A compact phase fluorimeter LUMOS developed in our lab[24] was used to measure the phosphorescence lifetime. It is equipped with an excitation LED (405 nm), short-pass filter (BG 12), a photodiode and a reference LED for phase correction. In the original configuration, a long-pass RG-630 filter (Schott) is positioned in front of the photodiode. This configuration was used to interrogate the chips modified with Type 1 nanoparticles. For the read-out of the chips modified with Type 2 particles the RG-630 filter was substituted by an RG-9 filter (Schott). The decay times τ were calculated from the luminescence phase shifts Φ according to: $\tau = tan\, \Phi / (2\pi f)$, where f is the modulation frequency. It was 3 kHz for both types of the nanoparticles.

Phosphorescence lifetime imaging

Phosphorescence lifetime imaging was performed with a gateable monochrome camera (PCO Sensicam, PCO, Kelheim, Germany) equipped with a Schneider-Kreuznach Xenoplan 1.4/23-0902 (www.schneiderkreuznach.com) lens using the 2-window rapid lifetime determination scheme.[25] Excitation was performed with the light of a 458 nm high power 10 W LED array (www.led-tech.de) filtered through a BG 12 filter (Schott).

Ratiometric intensity imaging

Ratiometric imaging was performed using a dual chip RGB-NIR camera (Jai AD-130GE) equipped with Pentax TV lens 12 mm or Schneider-Kreuznach Xenoplan 1.4/23-0902 lenses and the software described previously.[26] Excitation was performed with the light of a 458 nm high power 10 W LED array filtered through a BG 12 filter. A long-pass OG 515 glass filter (Schott) was used in front of the camera.

Response time and repeatability of the sensors

A powder blasted glass spot was modified with nanoparticles of Type II using the procedure described for modification of powder-blasted chips. It was glued on the inner wall of a 1 cm glass cuvette. The luminescence intensity was recorded in the kinetic mode on a Fluorolog (Horiba Jobin Yvon) fluorescence spectrometer (excitation 450 nm, emission 780 nm). To assess the repeatability of the sensor response, successive sensing cycles were performed using compressed air and nitrogen.

The LUMOS device was used to investigate the dynamic response in the aqueous phase. A glass piece (~ 1 x 1 cm) modified according to the procedure described for powder-blasted/smooth chips was glued on a bottom of a glass vial and the luminescence was read out through the vial bottom. The surface of the glass was covered with a thin (~ 1 cm) layer of air-saturated water, after which an excess of the anoxic solution (5% wt. glucose and 0.5% wt. glucose oxidase) was rapidly added into the vial.

Sensor coating stability tests

The microfluidic chips were continuously flushed with different pH buffers (acetate, MES and CHES with pH = 4, 6 and 8.9, respectively; 20 mM of buffer, total ionic strength 150 mM,

adjusted with sodium chloride) and also with the same buffers containing 1% of PEG 6000. The emission intensity and decay time were monitored in the frequency domain.

Calibration in gas phase and in water

Calibration mixtures were produced by mixing nitrogen (5.0, Linde Gas) and compressed air using a computer-controlled gas mixing device (Red-y smart series, Vögtlin Instruments). For calibration in water a glass piece (~ 1 x 1 cm) modified according to the procedure described for powder-blasted/smooth chips was positioned inside a glass vial and the gas mixtures were bubbled through the rubber septum. An adapted version of the Stern-Volmer equation from the two-site model,[27] which formally assigns the sensor molecules to two different micro-environments within the polymer, with different oxygen permeabilities, was used to fit the calibration plots:

$$\frac{I_0}{I} = \frac{\tau_0}{\tau} = \left(\frac{f}{1 + K_{SV} \cdot [O_2]} + \frac{1 - f}{1 + K_{SV} \cdot m \cdot [O_2]} \right)^{-1}$$

where K_{sv} describes the quenching efficiency for the first environment, f is the distribution coefficient between the two media and m is the factor defining the Stern-Volmer constant for the second environment.

In case of microfluidic chips a two point calibration was performed using air-saturated water and anoxic aqueous solution of 5% wt. glucose and 0.1% wt. of glucose oxidase (from *Aspergillus niger*, 192 U mg^{-1}, Sigma Aldrich).

Data evaluation

The calibration plots were fitted using the Origin 8.6 software from OriginLab (www.originlab.com). Original images were converted to false color oxygen distribution images in Matlab (www.mathworks.com) on the basis of respective calibration data.

Investigation of enzymatic activity in packed-bed reactors

Silica beads (∅ 100 µm) containing glucose oxidase immobilized by physical adsorption were packed inside the reactor through the largest central inlet. The inlet was sealed and the chip was fixed in a home-made chip holder. A 5% wt. aqueous solution of glucose was guided through the

chip at different flow rates using a programmable syringe pump (TSE systems GmbH, www.tse-systems.com). The read-out was performed with the LOMOS device.

Demonstration of oxygenation gradients in solution

A meander chip (∅ 0.15 mm) with integrated oxygen sensor was fixed in a home-made holder with the two inlets connected to programmable syringe pumps (TSE systems). Air-saturated aqueous solutions of glucose (1% wt.) in a phosphate buffer (pH 7) and glucose oxidase (0.005% wt.) in phosphate buffer pH 7 were injected simultaneously into the chip.

Results and discussion

1. Integration of oxygen sensors in rough surface glass-based microfluidics

A novel strategy of the integration of optical oxygen sensors into microfluidic chips is schematically depicted in Fig. 1a. It relies on physical adsorption of oxygen-sensitive nanoparticles on the glass surface. A channel of the chip is filled with an aqueous dispersion of the nanoparticles, incubated overnight and thoroughly washed with water to remove the non-adsorbed nanoparticles. Evidently, this is an extremely simple and convenient strategy which does require multiple steps needed so far for modification and assembling of glass chips.

Properties of the nanoparticles are of crucial importance for their deposition on the surface of the channels and subsequent application for oxygen sensing. It is essential that the nanoparticles possess good adhesion to glass and show bright luminescence which is modulated by oxygen. Recently reported conjugated polymer nanoparticles[23] combine all these properties. They include a hydrophobic polyfluorene (Type I, Fig. S1) or a poly(fluorene-co-benzothiadiazole) (Type II) backbone containing covalently grafted Pt(II) (benzo)porphyrins. The conjugated polymer can be viewed as a pure chromophore which efficiently absorbs violet or blue light and thus acts as a light-harvesting antenna (Fig. S2). This is in contrast to the commonly used dye-doped nanoparticles that contain only small dye amounts (several wt. %) dissolved in an optically silent polymer. Thus, even thin layer of the conjugated polymer nanoparticles can produce sufficient luminescence output. Importantly, the excitation energy is transferred to the Pt(II) porphyrin which shows oxygen-dependent emission in the red (Type I, Fig. S2) or NIR (Type II) parts of the spectrum. It should also be mentioned that the conjugated polymer nanoparticles bear both positively- and negatively-charged functional groups

(dominated by positively charged quaternary ammonium groups, Fig. S1) which not only ensure their dispercibility in aqueous media but may also be responsible for the excellent adhesion on negatively-charged glass surface.

As can be visible from the scanning electron microscopy (SEM) images (Fig. 1 B), the powder-blasted glass has a rough surface with many indentations and cracks. The surface area of the powder-blasted glass is thus much higher than that of the smooth glass. Efficient deposition of the conjugated polymer nanoparticles on the glass surface is evident (Fig. 1C and D). In many areas of the surface the nanoparticles form agglomerates which form layers several hundred nanometers thick. Considering the light-harvesting effect of the conjugated polymer, the layers are thick enough to generate sufficient luminescence signal. For comparison, the conventional sensing materials would require layers of several μm in thickness to achieve efficient luminescence. The size of the individual nanoparticles in the agglomerates (Fig. 1D) correlates well to the size of the beads obtained in a TEM measurement (Fig. 1E), which is about 25-35 nm. Comparison of the SEM images obtained with an In-Lens and BSE detector (Fig. S3) reveals high concentration of organic matter in the areas of agglomerates (BSE image) compared to the areas of glass containing no agglomerates but rather a mono-layer of the nanoparticles.

It is assumed that efficient adsorption of the nanoparticles on glass is due to the interaction between the positively-charged groups of the nanobeads and the negatively-charged glass surface. The agglomeration itself can be due to the combination of efficient interaction between the positively- and negatively-charged groups of different nanoparticles but also because of the π-π interaction between the aromatic backbone of the polymer which is essentially hydrophobic. It is also likely that the cracks and cavities of the powder blasted chips not only increase the surface area but also provide the anchoring points for the agglomerates.

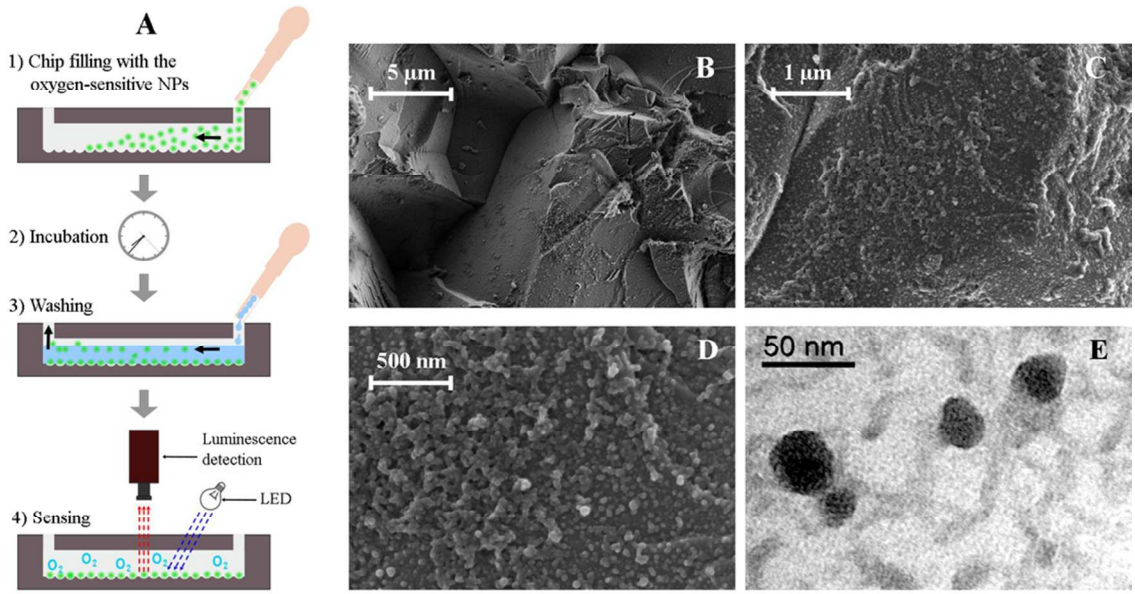

Fig. 1. Integration of oxygen sensors into powder-blasted glass microchannels. A: Schematic representation of the procedure based on physical adsorption of the oxygen-sensitive conjugated polymer nanoparticles; B-D: Scanning electron microscopy images (In-Lens detector) of the powder blasted glass surface modified with the nanoparticles; E – Transmission electron microscopy images of the nanoparticles.

2. Modification of smooth glass surfaces

As was demonstrated above, rough glass surfaces do not require any modification prior to immobilization of the oxygen-sensitive nanoparticles. However, the adsorption of the nanoparticles on polished glass surfaces was too poor to enable sufficient signal intensities. Etching of glass with hydrofluoric is a popular method,[28] however we found it difficult to obtain homogeneous surfaces inside the microfluidic channels. Here we propose a simple technique for modification of smooth glass surfaces which relies on *in-situ* generation of silica microparticles and their deposition on the bottom of a microfluidic channel (Fig. 2A). Although previous reports use similar deposition methods, they either require subsequent sintering at high temperature (450 °C)[29] or coating of the glass surface with positively charged polyelectrolytes to promote electrostatic attraction.[30,31] In the very simple procedure described here, the chip is filled with acidic aqueous solution of TEOS, incubated for 20-30 min to promote formation and deposition of the microparticles, washed with water and dried. Hydrolysis of tetraethyl orthosilicate (TEOS) resulting in formation of silicon oxide can be catalized by acids and

bases.[32,33,34] In order to obtain dense microparticles it is necessary to use an acid catalyst like acetic acid since basic hydrolysis typically results in a formation of a gel. As can be seen, the smooth surface of the chip (Fig. 2B) becomes rough after modification (Fig. 2C). SEM images (Fig.s 2D and E) provide the insight on the morphology of the microparticles. They are very uniform with the diameter of about 2 µm. The microparticles are covalently bound to each other but also to the surface of the chip where a thin layer of silica is deposited (Fig. 2D).

Integration of the oxygen-sensitive nanoparticles onto the modified surface is performed using the same procedure as described for the powder-blasted chips. A dramatic improvement of the luminescence signal is evident for the pack-bed reactors modified with silica microparticles compared to the not modified ones (Fig.s 2F and G).

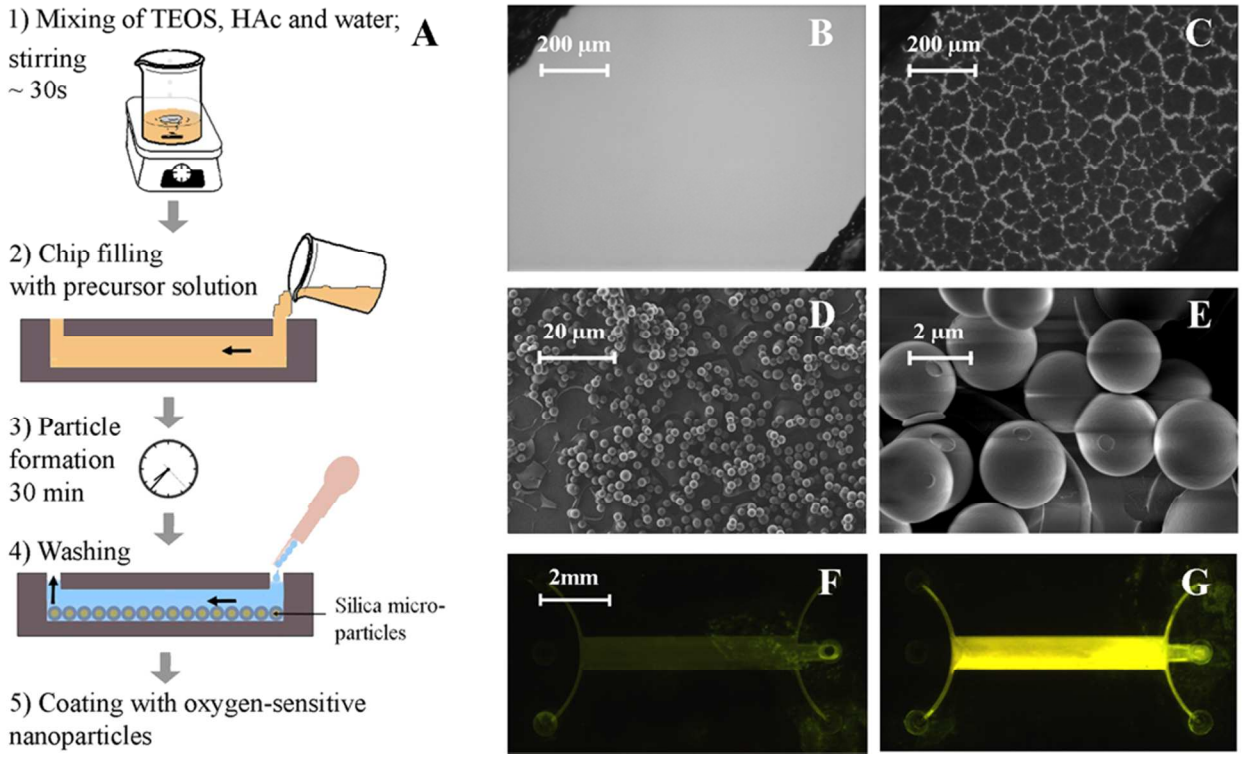

Fig. 2. Functionalization of smooth glass surface of the microchannels with silica microparticles. A: Schematic representation of the procedure based on in situ generation and deposition of the silica microparticles using a sol-gel technique; B and C: Optical microscopy images of a microchannel before (B) and after (C) modification; D and E: Scanning electron microscopy images of the silica microparticles deposited on a smooth glass surface; F and G: Intensity images (green channel, dual chip camera, 465 nm excitation) acquired for the packed-bed reactors with integrated oxygen sensors (Type II nanoparticles) with original smooth surface (F) and modified with silica microparticles (G).

3. Oxygen-sensing capabilities of the modified chips

Fig. 3 shows the Stern-Volmer plots for the sensors integrated onto powder-blasted and silica-modified surfaces, both for gas phase and liquid phase. The Stern-Volmer plots are non-linear, which is, however, a typical case for most oxygen sensors.[27] Such behavior can be described by so called "two site model", which assumes localization of the oxygen indicator in two different environments, possessing significantly different oxygen permeabilities. Although the model is physically meaningful only for the luminescence intensity, the equation (experimental part) can be also used to fit the decay time plots. For all the materials, quenching is less efficient in the aqueous media than in the gas phase. Simultaneously, Stern-Volmer plots show lower degree of non-linearity in the gas phase compared to those obtained for the aqueous media. This can be explained by more inhomogeneous environment present in the gas phase: some indicator molecules may not be completely surrounded by the conjugated polymer and are directly exposed to air, where oxygen quenching ability is very high. In fact, some of the most sensitive oxygen sensors reported rely on the indicators bounded to the surface of silica-gel and exposed to air.[35] Evidently, the adsorbed nanoparticles possess more homogeneous environment in water.

It can also be observed that the nanoparticles adsorbed on the silica-modified glass are more sensitive to oxygen that those adsorbed on the powder-blasted surface. Finally, comparison of the two different conjugated polymers reveals that the sensitivity of the sensors based on the Type I system is higher in all cases than the sensitivity of the sensors based on the Type II conjugated polymer. It is attributed to the longer luminescence decay time of the non-extended Pt(II) porphyrin in the Type I (τ_0 = 39 and 41 μs for the powder-blasted and silica-modified surfaces in gas, respectively) compared to the decay time of Pt(II) benzoporphyrin used in the Type II system (τ_0 = 21 and 30 μs for the powder-blasted and silica-modified surfaces, respectively). It should be mentioned here that it is possible to substitute the Pt(II) porphyrins in the conjugated polymer via Pd(II) porphyrins (which have 7-10 fold longer decay times) and thus to drastically increase the sensitivity of the resulting sensors. The materials based on the Pt(II) indicators cover the dynamic range from 0.1 kPa of O_2 to the concentrations exceeding air saturation, which is optimal for most applications. However, they are poorly suitable for oxygen quantification in hypoxic conditions which are typical e.g. for tumours and tumour spheroids.[36,37] The sensors based on Pd(II) dyes are expected to have the dynamic range of 0.01-4 kPa and thus be much better suitable for such studies.

The Stern-Volmer plots presented above were acquired in the frequency domain using a LUMOS device. However, it is possible to use other read-out schemes to interrogate the sensors, e.g. a dual RGB/NIR chip camera for the read-out of Type II sensors. A gated CCD Sensicam camera[25] which proved to be an excellent tool in applications varying from microfluidics to marine biology[38,39] can be used for imaging of lifetime (and consequently oxygen) distribution of the modified chips (Fig. S4).

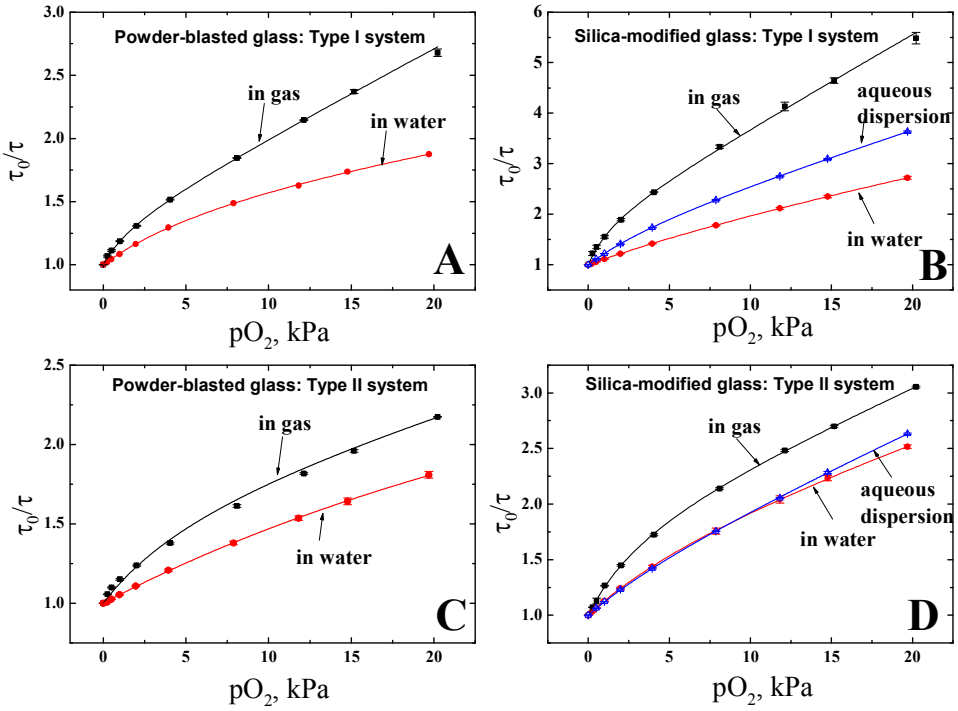

Fig. 3. Stern-Volmer plots for the oxygen sensors integrated onto the powder blasted (A and C) and silica microparticles-modified (B and D) glass for Type I (A and B) and Type II (C and D) conjugated polymers. Measurements in air (black curves) and water (red curves) for the integrated sensors and for the aqueous dispersion of the nanoparticles (blue curves) were performed with a LUMOS device at 22 °C.

4. Response time and repeatability

Dynamic response is a very important property of a sensing material. Whereas the nanoparticles respond virtually in real-time due to their small size and diffusion of the analyte from all the direction, the situation is completely different in the case of bulk sensing layer. In fact, a typical oxygen sensor based on a several µm-thick polymeric layer will respond to changes in analyte concentration between 2 and 30 seconds. Fast response was expected for the integrated sensors

since the deposition of the nanoparticles results in rather thin layers. Indeed, the response in the gas phase is very fast (Fig. 4A). The estimated response time < 0.2s is likely to be limited by the time needed to substitute the gasses in a flow chamber. The sensor shows repeatable behavior between the alternating cycles of air and nitrogen (Fig. 4B). It should be mentioned here that continuous measurement at high light intensities results in noticeable drift in the calibration due to photobleaching, therefore the setting should be chosen carefully to avoid unnecessary exposure to the strong light. Typically, a short light pulse of 10ms in duration (typical setting e.g. in LUMOS device) is sufficient to acquire a measurement point and thousands of measurements can be performed without any drift due to photobleaching.

Fig. 4C shows the response of the integrated sensors in the aqueous phase. The response of the sensors based on powder-blasted glass is as fast as in the gas phase (< 0.25 s) for the Type I and Type II nanoparticles. On the other hand, the response of the sensors based on silica-modified glass is definitely longer. The t_{90} (the time needed for 90% of the signal change to occur) was determined to be 0.8 and 2s for the sensors based on Type I and Type II nanoparticles, respectively. Nevertheless, the response is fast enough for virtually all potential applications.

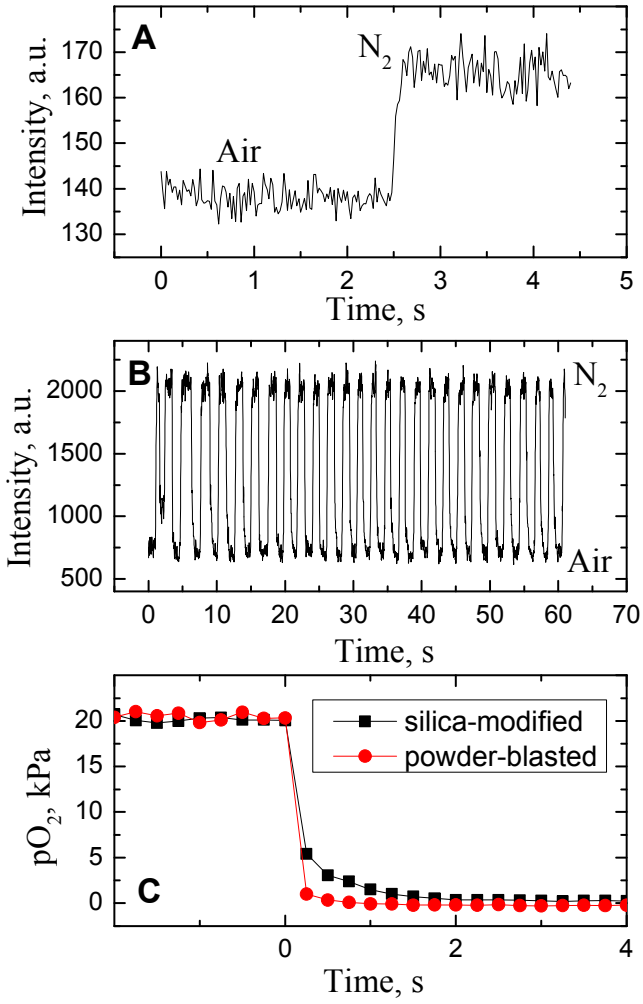

Fig. 4. Dynamic response (A) and repeatability (B) of the oxygen sensors integrated onto powder-blasted glass surface in the gas phase. C: dynamic response of the sensors based on powder-blasted and silica-modified surfaces in aqueous solution. In all the experiments, Type I nanoparticles were used.

5. Stability of the sensing layer

Since the integration of oxygen sensors relies on physical adsorption, the stability of the resulting layer may be critical due to desorption of the nanoparticles. Particularly, the stability may vary at different pH since the surface charge of the nanoparticles is pH dependent due to presence of carboxylic groups. Luckily, we could not observe any leaching of the adsorbed nanoparticles (indicated by the nearly constant luminescence intensity) during continuous pumping of the

buffer solutions (pH 4, 6, 9) through the microfluidic chip (Fig. S5A). The addition of surfactant (1% PEG-6000) to the buffer solutions did not affect the stability either (Fig. S5B).

6. Imaging of oxygen distribution

In order to demonstrate the potential of the new method in combination with monitoring oxygen concentration along a microfluidic channel, we choose a meander chip with channel diameter of 150 μm (Fig. 5). The chip was modified with the oxygen-sensing nanoparticles of Type II in order to enable ratiometric 2-wavelength read-out with a dual chip RGB/NIR camera. Recently we demonstrated that this affordable compact camera represents an excellent tool for the referenced read-out of optical sensors.[26] Thus, compared to rather popular imaging of optical sensors with RGB cameras, [40,41,42] the new tool significantly broadens the frontiers due to additional NIR channel. Fig. 5A shows that the emission of the Type II conjugated polymer nanoparticles almost perfectly matches the sensitivity of the green and NIR channels of the dual chip camera. Deoxygenation results in great enhancement of the phosphorescence from the Pt(II) benzoporphyrin visible solely in the NIR channel. On the other hand, the residual emission from the conjugated polymer antenna (green channel) is not affected by oxygen. Thus, the luminescence intensity ratio (NIR/green) serves as referenced parameter which enables compensation for variations in light intensity and inhomogeneities of the sensing layer. It should be mentioned here that the choice of the lens is critical for reliability of the measurement. For example, if the magnification is rather low and the whole chip is imaged (as shown in Fig. 5) the channel width corresponds to only 4 pixels. Thus, even a small misalignment between the RGB and NIR channel (not compensated by a normal lens but only by a chromatic aberration corrected one) can result in artefacts. This can be overcome by imaging of only a part of the chip or by using microfluidic chips with larger channel diameter as shown in Fig. S6.

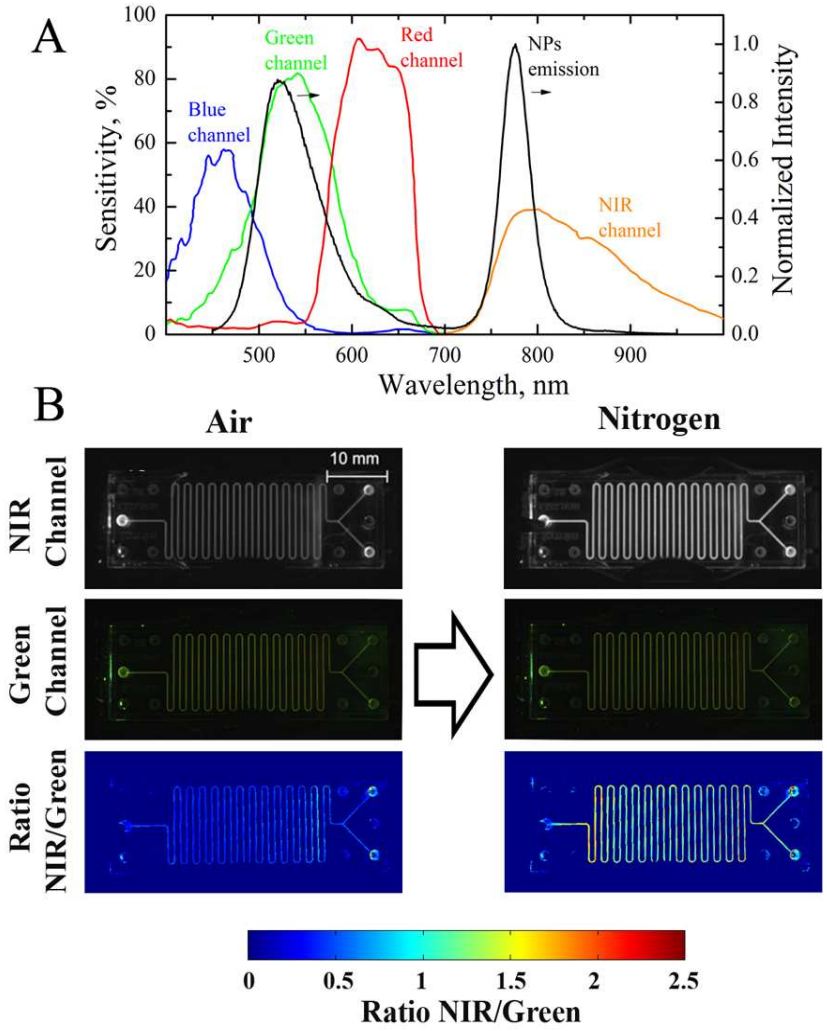

Fig. 5. Ratiometric imaging of oxygen in powder-blasted meander chips modified with oxygen-sensitive particles of Type II. A: The uncorrected emission spectrum of the nanoparticles and the spectral sensitivity of the channels of the dual chip RGB/NIR camera. B: From top to bottom: luminescence intensity images for the NIR and green channels and false color ratiometric NIR/green images of the integrated microfluidic oxygen sensor under air (left) and nitrogen (right).

7. Monitoring of enzyme activity in packed-bed microreactors

The scope of potential applications of the integrated chips is rather large.[14] Glass chips are particularly suitable for precise quantification of oxygen due to excellent gas-barrier properties of glass. In fact, the diffusion of the analyte through the chip material is virtually absent, which is

not the case for polymeric chips, particularly made of highly gas-permeable polymers.[43] Thus even rather slow red-ox processes can be investigated with help of modified chips. Fig. S7 shows that it is possible to monitor red-ox reactions (demonstrated for glucose oxidase-catalysed oxidation of glucose) even with the meander chips with 150 μm width channels. Of course, the limitations described above, (artefacts resulting from low resolution if the whole chip is viewed) should be considered here.

Packed-bed reactors with integrated oxygen sensors represent another very versatile tool to perform biocatalytic conversions in continues mode.[44,45] The potential of the integrated chips for continuous monitoring of an enzymamtic conversion in the micro-reactors is demonstrated. The microreactors (Fig. 6A) were filled with silica beads (∅ 100 μm) containing immobilized glucose oxidase (Fig. 6B). The outlet of the reactor is small enough for the silica beads to be retained, so that air-saturated aqueous solutions of glucose can be pumped through the reactor (Fig. 6A). A LUMOS device was used for sensor read-out; the calculated pO_2 is plotted in Fig. 6C. The system is very sensitive to changes in the flow rate of the glucose solution and the plateaus obtained reflect the equilibrium between the oxygen consumption during the enzymatic reaction and the oxygen introduced with the air-saturated glucose solution. If the flow is stopped, the solution rapidly becomes anoxic and the deoxygenation rate reflects the enzymatic activity and the enzyme loading onto the microbead carrier. We believe that the new integrated sensors represent an excellent tool for studying the enzymatic activity of red-ox enzymes and for investigation of immobilization strategies of the enzymes on particle carriers. Another remarkable feature of this system, apart from its simplicity and versatility, is that the reactor can be reused multiple times since the enzyme-carrying silica particles can be removed by a strong flow of water introduced in the outlets.

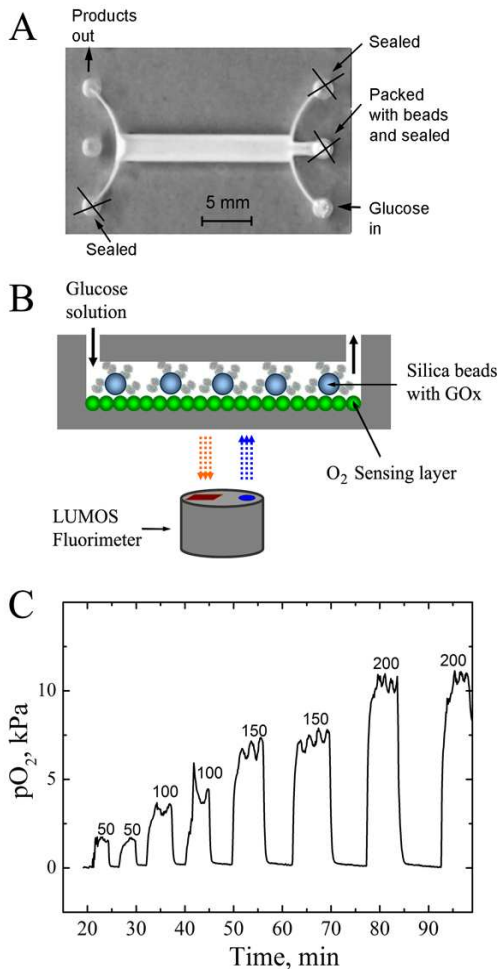

Fig. 6. Monitoring of enzymatic activity in packed-bed reactors with integrated oxygen sensors. A: Photographic image of the reactor; B: Schematic representation of the experimental setup; C: Real-time monitoring of oxygen concentration inside the reactor at different flow rates (µl/min).

Conclusions

We presented a novel technique for integration of optical oxygen sensors into microfluidic glass chips. The simple technique relies on physical adsorption of oxygen-sensitive conjugated polymer nanoparticles which produce sensing layers of exceptional properties (excellent stability, very fast response, optimal sensitivity and suitability for the read-out in ratiometric and lifetime modalities).

We also developed a simple and efficient strategy for increasing the surface area of smooth glass surfaces by *in-situ* generation and deposition of silica microparticles making them suitable adsorbents for the oxygen-sensitive nanoparticles. The microparticles may also be suitable for

integrating sensors for other analytes (such as pH) by e.g. covalently coupling of the indicators to the surface of the beads. This can further expand the range of possible applications of the integrated sensors.

Similarly to the use of magnetic sensing particles, the new strategy allows integration of the oxygen sensors in already assembled chips, but does not require a magnet. This is in contrast to the state-of-the-art techniques which require closing of the chip after integration of the sensors. Clearly, the new method is applicable to modification of other glass surfaces (spots, capillaries etc.) which substantially extends the scope of potential applications. However, this is also the main limitation of the method, since the plastic-based materials cannot be modified. Nevertheless, we believe that the glass microfluidic chips and reactors with integrated oxygen sensors represent promising tools for quantification of oxygen in air and aqueous environment and particularly for investigation of different red-ox bioprocesses.

Acknowledgements

Financial support from the European Union FP7 (Project BIOINTENSE, N. 312148), CONICET (L.C. Lasave postdoctoral fellowship) is gratefully acknowledged. We also thank Dr. Juan Manuel Bolivar Bolivar (Graz University of Technology) for providing the silica microbeads with immobilized glucose oxidase.

References

1 N. Wang, X. Zhang, Y. Wang, W. Yuc and H. L. W. Chan, *Lab Chip*, 2014, **14**, 1074-1082.

2 D. B. Papkovsky and R. I. Dmitriev, *Chem. Soc. Rev.*, 2013, **42**, 8700-8732.

3 E. K. Sackmann, A. L. Fulton and D. J. Beebe, *Nature*, 2014, **507**, 181-189.

4 Y. Guo, X. Li, S. Ye and S. Zhang, *TrAC-Trend. Anal. Chem.*, 2013, **42**, 168-185.

5 A. Bange, H. B. Halsall and W. R. Heineman, *Biosens. Bioelectron.*, 2005, **20**, 2488-2503.

6 R. Monošík, L. Angnes, *Microchem. J.*, 2015, **119**, 159-168.

7 P. N. Nge, C. I. Rogers and A. T. Woolley, *Chem. Rev.*, 2013, **113**, 2550-2583.

8 E. Elizalde, R. Urteaga and C. L. A. Berli, *Lab Chip*, 2015, **15**, 2173-2180.

9 X. Wang and O. S. Wolfbeis, *Chem. Soc. Rev.*, 2014, **43**, 3666-3761.

10 M. Quaranta, S. M. Borisov and I. Klimant, *Bioanal. Rev.*, 2012, **4**, 115–157.

11 J. W. Grate, R. T. Kelly, J. Suter and N. C. Anheier, *Lab Chip*, 2012, **12**, 4796-4801.

12 A. Han, H. Hou, L. Li, H. S. Kim and P. de Figueiredo, *Trends Biotechnol.*, 2013, **31**, 225-232.

13 P. C. Thomas, M. Halter, A. Tona, S. R. Raghavan, A. L. Plant, und S. P. Forry, *Anal. Chem.*, 2009, **81**, 9239–9246

14 S. Sun, B. Ungerböck and T. Mayr, *Methods Appl. Fluoresc.*, 2015, **31**, 034002.

15 V. Nock, R. J. Blaikie, and T. David, *Lab Chip*, 2008, **8**, 1300–1307.

16 L. Gitlin, C. Hoera, R. J. Meier, S. Nagl, and D. Belder, *Lab Chip*, 2013, **13**, 4134–4141.

17 S. M. Grist, N. Oyunerdene, J. Flueckiger, J. Kim, P. C. Wong, L. Chrostowski, and K. C. Cheung, *The Analyst*, 2014, **139**, 5718–5727.

18 J. R. Etzkorn, W.-C. Wu, Z. Tian, P. Kim, S.-H. Jang, D. R. Meldrum, A. K.-Y. Jen, and B. A. Parviz, *J. Micromech. Microeng.*, 2010, **20**, 095017.

19 C. Herzog, E. Beckert, and S. Nagl, *Anal. Chem.*, 2014, **86**, 9533–9539.

20 A. R. Thete, G. A. Gross, and J. M. Koehler, *Analyst*, 2009, **134**, 394–400.

21 B. Ungerböck, V. Charwat, P. Ertl and T. Mayr, *Lab Chip*, 2013, **13**, 1593–1601.

22 B. Ungerböck, P. Sulzer, S. Fellinger, T. Abel and T. Mayr, *Analyst*, 2014, **139**, 2551-2559.

23 R. I. Dmitriev, S. M. Borisov, H. Dussmann, S. Sun, B. J. Müller, J. Prehn, V. P. Baklaushev, I. Klimant and D. B. Papkovsky, *ACS Nano*, 2015 **9**, 5275–5288.

24 P. Lehner, C. Larndorfer, E. Garcia-Robledo, M. Larsen, S. M. Borisov, N. P. Revsbech, R. N. Glud, D. E. Canfield and I. Klimant, *PLOS ONE*, 2015, **10**, e0128125.

25 G. Holst and B. Grunwald, *Sensor. Actuat. B-Chem.*, 2001, **74**, 78–90.

26 J. Ehgartner, H. Wiltsche, S. M. Borisov and T. Mayr, *Analyst*, 2014, **139**, 4924-4933.

27 E. R. Carraway, J. N. Demas, B. A. DeGraff and J. R. Bacon, *Anal. Chem.*, 1991, **63**, 337–342.

28 G. A. C. M. Spierings, *J Mater Sci*, 1993, **28**, 6261–6273.

29 P. S. Tsai, Y. M. Yang, and Y. L. Lee, *Langmuir*, 2006, **22**, 5660–5665.

30 B. T. Liu and W. D. Yeh, *Colloids Surf., A*, 2010, **356**, 145–149.

31 X. Li and J. He, *ACS Appl. Mater. Interfaces*, 2013, **5**, 5282–5290.

32 B. Karmakar, G. De and D. Ganguli, *J. Non-Cryst. Solids*, 2000, **272**, 119-126.

33 G. De, B. Karmakar and D. Ganguli, *J. Mater. Chem.*, 2000, **10**, 2289-2293.

34 C. Moran, G. Hale and N. Halas, *Langmuir*, 2001, **17**, 8376-8379.

35 S. M. Borisov, P. Lehner and I. Klimant, *Anal. Chim. Acta*, 2011, **690**, 108–115.

36 P. Vaupel und L. Harrison, *The Oncologist*, 2004, **9**, 4–9.

37 D. R. Grimes, C. Kelly, K. Bloch, und M. Partridge, *J. R. Soc. Interface*, 2014, **11**, 20131124.

38 B. Ungerböck, A. Pohar, T. Mayr and I. Plazl, *Microfluid. Nanofluid.*, 2012, **14**, 565–574.

39 M. Kühl, L. F. Rickelt and R. Thar, *Appl. Environ. Microbiol.*, 2007, **73**, 6289-6295.

40 R. J. Meier, L. H. Fischer, O. S. Wolfbeis, und M. Schäferling, *Sensors and Actuators B: Chemical*, 2013, **177**, 500–506.

41 X. Wang, R. J. Meier, M. Link, and O. S. Wolfbeis, *Angewandte Chemie International Edition*, 2010, **49**, 4907–4909.

42 M. I. J. Stich, S. M. Borisov, U. Henne, and M. Schäferling, *Sensor. Actuat. B-Chem.*, 2009, **139**, 204–207.

43 A. P. Vollmer, R. F. Probstein, R. Gilbert and T. Thorsen, *Lab Chip*, 2005, **5**, 1059-1066.

44 P. Fernandes, *Int. J. Mol. Sci.* 2010, **11**, 858–879.

45 R. Wohlgemuth, I. Plazl, P. Žnidaršič-Plazl, K. V. Gernaey, and J. M. Woodley, *Trends Biotechnol.* 2015, **33**, 302–314.

TOC Figure

A simple nanoparticle-based technique for integration of optical oxygen sensors in microfluidic glass chips